Lyman-alpha spectroscopy of extreme [O iii] emitting galaxies at z 2-3: implications for Lyα visibility and LyC leakage at z > 6

Mengtao Tang, Daniel Stark, Jacopo Chevallard, Stéphane Charlot, Ryan Endsley, Enrico Congiu

Monthly Notices of the ROYAL ASTRONOMICAL SOCIETY

MNRAS **503,** 4105–4117 (2021) doi:10.1093/mnras/stab705
Advance Access publication 2021 March 10

Lyman-alpha spectroscopy of extreme [O III] emitting galaxies at $z \simeq 2-3$: implications for Lyα visibility and LyC leakage at $z > 6$

Mengtao Tang [1,2]★ Daniel P. Stark,[1] Jacopo Chevallard [3] Stéphane Charlot,[3] Ryan Endsley [1] and Enrico Congiu [4,5]

[1]*Steward Observatory, University of Arizona, 933 N Cherry Ave, Tucson, AZ 85721, USA*
[2]*Department of Physics and Astronomy, University College London, Gower Street, London WC1E 6BT, UK*
[3]*Sorbonne Université, UPMC-CNRS, UMR7095, Institut d'Astrophysique de Paris, F-75014, Paris, France*
[4]*Departamento de Astronomía, Universidad de Chile, Camino del Observatorio 1515, Las Condes, Santiago, Chile*
[5]*Las Campanas Observatory, Carnegie Institution for Science, Colina el Pino, Casilla 601, La Serena, Chile*

Accepted 2021 March 5. Received 2021 March 4; in original form 2020 December 8

ABSTRACT

Spectroscopic observations of massive $z > 7$ galaxies selected to have extremely large [O III] + Hβ equivalent width (EW ∼1500 Å) have recently revealed large Lyα detection rates, in contrast to the weak emission seen in the general population. Why these systems are uniquely visible in Lyα at redshifts where the intergalactic medium (IGM) is likely significantly neutral is not clear. With the goal of better understanding these results, we have begun a campaign with MMT and Magellan to measure Lyα in galaxies with similar [O III] + Hβ EWs at $z \simeq 2$–3. At these redshifts, the IGM is highly ionized, allowing us to clearly disentangle how the Lyα properties depend on the [O III] + Hβ EW. Here, we present Lyα EWs of 49 galaxies at $z = 2.2$–3.7 with intense [O III] + Hβ line emission (EW = 300–3000 Å). Our results demonstrate that strong Lyα emission (EW >20 Å) becomes more common in galaxies with larger [O III] + Hβ EW, reflecting a combination of increasingly efficient ionizing photon production and enhanced transmission of Lyα. Among the galaxies with the most extreme [O III] + Hβ emission (EW ∼1500 Å), we find that strong Lyα emission is not ubiquitous, with only 50 per cent of our population showing Lyα EW >20 Å. Our data suggest that the range of Lyα strengths is related to the observed ellipticity, with those systems that appear edge-on or elongated having weaker Lyα emission. We use these results to interpret the anomalous Lyα properties seen in $z > 7$ galaxies with extreme [O III] + Hβ emission and discuss implications for the escape of ionizing radiation from these extreme line emitting galaxies.

Key words: galaxies: evolution – galaxies: formation – galaxies: high-redshift – cosmology: observations.

1 INTRODUCTION

The reionization of hydrogen in the intergalactic medium (IGM) is thought to be driven by the radiation from the first luminous objects, including both massive stars and active galactic nuclei (e.g. Loeb & Barkana 2001; Robertson et al. 2013, 2015; Bouwens et al. 2015; Madau & Haardt 2015; Stark 2016; Dayal & Ferrara 2018). Therefore, studying the process of reionization offers key clues to investigate the history of cosmic structure formation. Over the last two decades, the timeline of reionization has been constrained by several observations. Planck measurement of the electron-scattering optical depth of the cosmic microwave background implies a mid-point reionization redshift of $z \simeq 7.7$ (Planck Collaboration VI 2018). Meanwhile, observations of the Lyα and Lyβ forests in high redshift quasar spectra suggest that reionization is nearly complete by $z \approx 6$ (e.g. Fan et al. 2006; McGreer, Mesinger & D'Odorico 2015).

Spectroscopic measurements of Lyα emission from star-forming galaxies provide a complementary probe of the IGM at $z \gtrsim 7$ (e.g. Dijkstra 2014), where the population of quasars becomes rare (Fan et al. 2001; Manti et al. 2017). Because of the resonant scattering of Lyα photons by neutral hydrogen, the damping wings of the neutral patches in the IGM should suppress the Lyα emission from galaxies in the reionization era (e.g. Miralda-Escudé 1998; Santos 2004; Mesinger & Furlanetto 2008), decreasing the fraction of sources showing prominent Lyα emission (e.g. Stark et al. 2010; Fontana et al. 2010) and the abundance of narrowband-selected Lyα emitters (e.g. Malhotra & Rhoads 2004; Hu et al. 2010; Ouchi et al. 2010; Kashikawa et al. 2011; Konno et al. 2014; Santos, Sobral & Matthee 2016; Ota et al. 2017). Over the last decade, significant effort has been invested in campaigns to measure the equivalent width (EW) distribution of Lyα emission over cosmic time. Spectroscopic observations (e.g. Fontana et al. 2010; Stark, Ellis & Ouchi 2011; Treu et al. 2013; Caruana et al. 2014; Pentericci et al. 2014; Schenker et al. 2014; Tilvi et al. 2014; Jung et al. 2018, 2020; Mason et al. 2019) have demonstrated that there is a downturn in the fraction of strong Lyα emitting galaxies at $z \gtrsim 6.5$ (the so-called Lyα fraction, $x_{Ly\alpha}$), consistent with expectations for a significantly neutral IGM ($x_{HI} \gtrsim 0.5$) at $z \sim 7$ (e.g. Mesinger et al. 2015; Zheng et al. 2017; Mason et al. 2018, 2019; Hoag et al. 2019; Whitler et al. 2020; see Ouchi, Ono & Shibuya 2020, for a review).

★ E-mail: tangmtasua@email.arizona.edu

In the last several years, attention has focused on observations of four of the most luminous ($H_{160} = 25.0-25.3$) known galaxies at $z = 7$–9 (Roberts-Borsani et al. 2016, hereafter RB16). The red *Spitzer*/IRAC [3.6] − [4.5] colours of these four systems imply extremely large [O III] + Hβ[1] EWs ($\simeq$ 900–2000 Å), roughly twice the average [O III] + Hβ EW at $z \sim 7$–8 ($EW_{[O\,III]+H\beta} \simeq 670$ Å; Labbé et al. 2013; De Barros et al. 2019; Endsley et al. 2021a). All four galaxies exhibit strong Ly α emission at $z > 7$ (Oesch et al. 2015; Zitrin et al. 2015, RB16; Stark et al. 2017), implying a 100 per cent detection rate at redshifts where the IGM is expected to be mostly neutral. Taken together with two other similar $z > 7$ extreme [O III] emitters in the literature (Ono et al. 2012; Finkelstein et al. 2013), these detections imply an Ly α emitter fraction that is five times larger than what is seen in the general population at $z \sim 7$–8 (Stark et al. 2017). Why this population presents such strong Ly α emission is still a matter of debate. Some have suggested that these luminous systems trace overdense regions with larger-than-average ionized bubbles, boosting the transmission of Ly α through the IGM (e.g. Barkana & Loeb 2004; Endsley et al. 2021b). Alternatively, the large rest-frame optical line EWs of these galaxies may indicate hard ionizing radiation fields, potentially enhancing both the production efficiency and the escape fraction of Ly α photons through the galaxies (e.g. Stark et al. 2017).

One of the challenges of interpreting the emerging body of reionization-era spectra stems from limitations in our understanding of the galaxies with large [O III] + Hβ EWs (=300–3000 Å). While this population is common at $z > 6$, they are rare among continuum-selected samples at lower redshifts. Fortunately, a series of observational campaigns have begun to identify large samples of extreme [O III] emitting galaxies at $z \simeq 0$ (e.g. Cardamone et al. 2009; Senchyna et al. 2017; Yang et al. 2017b), $z \simeq 1$ (e.g. Atek et al. 2011; Amorín et al. 2014, 2015; Huang et al. 2015), and $z \simeq 2$–3 (e.g. van der Wel et al. 2011; Maseda et al. 2014; Forrest et al. 2017), opening the door for detailed spectroscopic studies of galaxies with similar properties to those at $z > 6$ (e.g. Labbé et al. 2013; Smit et al. 2015; Roberts-Borsani et al. 2016; De Barros et al. 2019; Endsley et al. 2021a). In Tang et al. (2019, hereafter T19), we presented results from a large near-infrared spectroscopic campaign targeting rest-frame optical emission lines in $z \simeq 2$ galaxies with [O III] EW = 300–2000 Å. The combination of dust-corrected Hα and far-UV continuum luminosities enabled calculation of the ionizing photon production efficiency ($\xi_{\rm ion}$), defined as the ratio of the production rate of hydrogen-ionizing photons ($N_{\rm ion}$) and the UV luminosity at 1500 Å ($L_{\rm UV}$, including nebular and stellar continuum) corrected for dust attenuation from the diffuse interstellar medium (ISM). As had been shown previously in nearby galaxy samples (Chevallard et al. 2018), T19 found that $\xi_{\rm ion}$ scales with the [O III] EW, reaching very large values in the most extreme line emitters. The ionization state and dust content of the nebular gas are also found to scale with [O III] EW, such that the most intense [O III] emitters tend to have gas that is both highly ionized and nearly dust-free. With efficient ionizing photon production and little dust, we expect that the production and escape of Ly α photons should be maximized (per $L_{\rm UV}$) in galaxies with the largest [O III] EW, potentially explaining the anomalous Ly α detection rates in the RB16 sample at $z > 7$. This general picture is supported by observations at $z \simeq 0$–1 (e.g. Cowie, Barger & Hu 2011; Amorín et al. 2015; Yang et al. 2017a), which suggest that intense [O III] emitting galaxies do indeed tend to exhibit large EW Ly α emission.

[1]In this paper, the [O III] in [O III] + H β refers to [O III] $\lambda\lambda$4959, 5007.

The next step is to investigate how the Ly α EW distribution varies over the full range of [O III] EWs expected in the reionization era, targeting galaxies at lower redshifts where the IGM is known to be highly ionized. Such a data set would reveal how factors internal to galaxies impact the emergent Ly α luminosity, providing an empirical baseline at high redshift that is independent of IGM attenuation. This goal has motivated observations of Ly α emission in $z \simeq 2$–3 galaxies selected to have intense [O III] emission in 3D-*HST* grism spectra (Momcheva et al. 2016). The first results were presented in Du et al. (2020), based on a survey conducted with Keck/LRIS. Surprisingly, the data revealed no significant correlation between Ly α and [O III] EWs for galaxies in the range 100 Å $\lesssim$ [O III] $\lambda\lambda$4959, 5007 EW $\lesssim$ 1000 Å. In this paper, we focus on extending the Ly α statistics to higher optical line EWs[2] ([O III] λ5007 EW $\gtrsim$ 1000 Å, or equivalently $EW_{[O\,III]+H\beta} \gtrsim 1500$ Å), with the aim of better understanding the Ly α detections in the $z > 7$ RB16 galaxies (median $EW_{[O\,III]+H\beta} \simeq 1500$ Å). The results presented in Du et al. (2020) suggest that stronger Ly α emission does indeed appear in this more extreme population, but samples are still small at high redshift, with only two [O III]-selected galaxies in the $EW_{[O\,III]\lambda5007} \gtrsim 1000$ Å (i.e. $EW_{[O\,III]\lambda\lambda4959,5007} \gtrsim 1333$ Å) regime. Here, we present new Ly α measurements for 49 $z \simeq 2$–3 galaxies with intense [O III] emission, including 11 with [O III] λ5007 EW $\gtrsim$ 1000 Å, enabling a factor of 5 improvement in Ly α statistics for the most extreme line emitters. With this statistical baseline in hand, we can begin to understand how factors internal to the galaxy (i.e. radiation field, transmission through the circumgalactic medium) impact the visibility of Ly α in the most intense [O III] emitters, providing new insight into what is likely to be driving the anomalous Ly α detection rates seen in similar systems at $z > 7$.

The organization of this paper is as follows. We describe the observations and Ly α spectra in Section 2. The Ly α spectroscopic properties of our extreme [O III] emitters at $z \simeq 2$–3 are presented in Section 3. We discuss the implications of the results for galaxies in the reionization era in Section 4 and summarize our conclusions in Section 5. We adopt a Λ-dominated, flat universe with $\Omega_\Lambda = 0.7$, $\Omega_{\rm M} = 0.3$, and $H_0 = 70$ km s^{-1} Mpc^{-1}. All magnitudes in this paper are quoted in the AB system (Oke & Gunn 1983), and all EWs are quoted in the rest frame.

2 OBSERVATIONS AND ANALYSIS

We aim to characterize the Ly α properties of galaxies with extremely large EW optical emission lines. The data were taken from our optical (rest-frame UV) spectroscopic survey of extreme [O III] emitters at $z = 1.3$–3.7 using the Inamori–Magellan Areal Camera & Spectrograph (IMACS; Dressler et al. 2011) on the Magellan Baade telescope and the Binospec (Fabricant et al. 2019) on the MMT telescope. Details of the sample selection and spectroscopic observations of this survey are described in Tang et al. (2021, hereafter T21). In this section, we briefly summarize the rest-frame UV spectroscopy in Section 2.1 and then present the Ly α emission line measurements in Section 2.2.

[2]Note that in Du et al. (2020), the [O III] EW refers to [O III] $\lambda\lambda$4959, 5007 EW while throughout this paper, we will use [O III] λ5007 EW and [O III] + H β EW. Adopting the theoretical flux ratio $I(5007)/I(4959) = 3$, we have $EW_{[O\,III]\lambda5007} = 3/4 \times EW_{[O\,III]\lambda\lambda4959,5007}$. Assuming the typical flux ratio of [O III] λ5007/Hβ = 6 measured for extreme emission line galaxies (e.g. Maseda et al. 2014, T19), we have $EW_{[O\,III]+H\beta} = 1.5 \times EW_{[O\,III]\lambda5007}$.

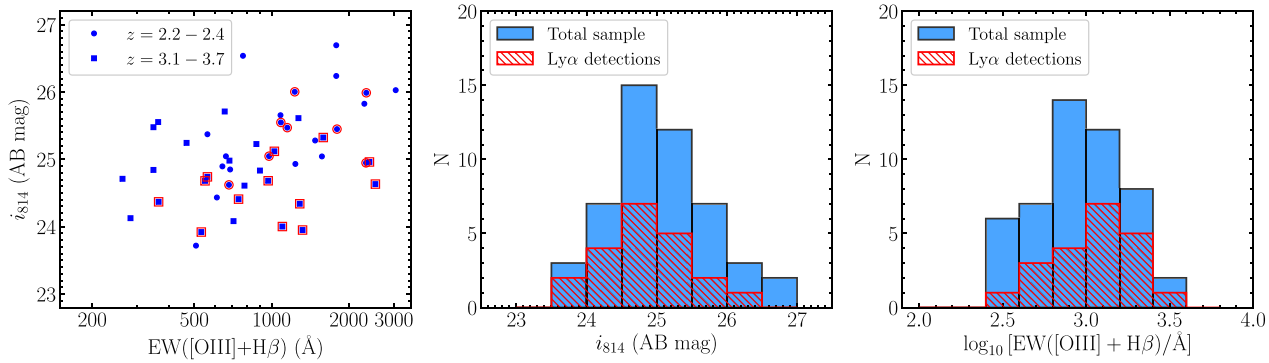

Figure 1. *HST* F814W magnitude (i_{814}) and [O III] + H β EW distribution of the 49 extreme [O III] emitters at z = 2.2–3.7 in our spectroscopic sample. Left-hand panel: F814W magnitudes versus [O III] + H β EWs of the 49 galaxies (objects at z = 2.2–2.4 are shown by blue circles and objects at 3.1−3.7 are shown by blue squares); sources with Ly α detections are marked by open red circles or squares. Middle panel: F814W magnitude distributions of the total extreme [O III] emitter sample (solid blue) and the subset with Ly α emission line detections (dashed red). Right-hand panel: [O III] + H β EW distributions of the total sample (solid blue) and the subset with Ly α detections (dashed red). Our sample spans a range of F814W magnitudes that goes from 24 to 27 AB mag, and a wide range of [O III] + H β EW (300–3000 Å), which are similar to the values expected at $z > 6$.

2.1 MMT/Binospec and Magellan/IMACS spectroscopy

The rest-frame UV spectra used in this work are presented in T21, which follow a large spectroscopic effort to obtain rest-frame optical spectra of extreme [O III] emitters at z = 1.3–3.7 (T19; Tang et al., in preparation). The sample of extreme [O III] emitters was identified based on the [O III] EWs inferred from *HST* grism spectra (at z = 1.3–2.4; T19) or the *K*-band flux excess (at z = 3.1−3.7; Tang et al., in preparation). We require the extreme [O III] emitters to have rest-frame [O III] λλ4959, 5007 EW ≃ 300–2000 Å, which are chosen to match the values expected to be common in reionization-era systems. Over three observing runs between 2018 and 2019, we have obtained rest-frame UV spectra for 138 extreme [O III] emitters with Magellan/IMACS and MMT/Binospec, targeting UV metal line emission (C IV λλ1548, 1550, O III] λλ1661, 1666, C III] λλ1907, 1909; T21) and Ly α. The Magellan/IMACS spectra were reduced using the Carnegie Observatories System for MultiObject Spectroscopy[3] pipeline (Dressler et al. 2011; Oemler et al. 2017), and the MMT/Binospec spectra were reduced using the publicly available Binospec data reduction pipeline[4] (Kansky et al. 2019). We performed the slit loss correction following the same procedures in T19, and the absolute flux calibration using observations of slit stars.

Our goal is to measure Ly α emission lines in extreme [O III] emitters. Due to the wavelength coverage (≃ 3900–9000 Å) of IMACS and Binospec spectra, Ly α is visible for galaxies at $z > 2.2$. There are 49 extreme [O III] emitters at $z > 2.2$ in our spectroscopic sample. We show the i_{814} magnitude and [O III] + H β EW distribution of these 49 sources in Fig. 1. The median i_{814} magnitude of our sample is 25.0. We derive the stellar population properties of the 49 galaxies by fitting the broad-band photometry and the available rest-frame optical emission line fluxes using the Bayesian spectral energy distribution (SED) modelling and interpreting tool BEAGLE (version 0.23.0; Chevallard & Charlot 2016). Details of the SED modelling procedures with BEAGLE and the results have been discussed in T21. In Fig. 2, we show the best-fitting stellar masses, specific star formation rates (sSFRs), and stellar ages (assuming constant star formation history) of the 49 sources. The median [O III] + H β EW (901 Å) and sSFR (52 Gyr^{-1}) of our sample are larger than those of typical $z \sim$ 7–8 galaxies (EW$_{[\rm O\,III]+\rm H\beta}$ ∼ 700 Å and sSFR ∼10 Gyr^{-1}; e.g. Labbé et al. 2013; De Barros et al. 2019; Endsley et al. 2021a) since we prioritize targets with the largest EWs (>1000 Å; T21). However, our sample still spans the full range of EWs expected at $z > 6$ (EW$_{[\rm O\,III]+\rm H\beta}$ ≃ 300–3000 Å; e.g. Stark 2016), allowing us to investigate how Ly α EW varies over the [O III] + H β EWs expected in the reionization era.

2.2 Emission line measurements

We identify Ly α emission lines from the 2D rest-frame UV spectra of the 49 extreme [O III] emitters at z = 2.2–3.7 by visually inspecting the expected positions of Ly α using the measured redshifts. For 27 sources in our sample, the redshifts were computed by fitting the [O III] λ5007 emission line from the ground-based (T19) or *HST* grism-based (Momcheva et al. 2016) near-infrared spectra. For the remaining 22 objects at z = 3.1−3.7 whose near-infrared spectra are not available, we rely on the photometric redshift measurements from Skelton et al. (2014). We detected Ly α emission lines with S/N >3 in 21 out of the 49 extreme [O III] emitters at z = 2.2–3.7 in our spectroscopic sample. For the 22 objects with photometric redshifts only, Ly α emission was detected in 8 (36 per cent) systems. The Ly α detection rate is higher in the subset with spectroscopic redshifts measured from [O III] λ5007 (13/27; 48 per cent).

Ly α emission line fluxes are determined from the 1D spectra (Fig. 3), which are extracted from 2D spectra using a boxcar extraction. Twenty of the 21 Ly α emitting galaxies show single Ly α emission line features, and the flux was derived by fitting the line profile with a single Gaussian function. The central wavelength recovered from this fit is used to calculate the Ly α redshift. The remaining Ly α emitter (COSMOS-17636) in our sample shows a double-peaked Ly α profile (Fig. 3), and we fit the emission line with a double-Gaussian function. The line flux is computed by summing the fluxes derived from each single Gaussian profile. For galaxies without S/N >3 Ly α emission line measurements, we consider the line as undetected and compute the 3σ upper limit of the line flux. Using the wavelength boundaries adopted in Kornei et al. (2010), we derive the 1σ Ly α flux by integrating the error spectrum in quadrature over rest-frame 1199.9–1228.8 Å. Since the throughput declines rapidly at the short wavelength end (<4500 Å) of IMACS and Binospec spectrographs, the sensitivity of detecting an Ly α emission line in

[3] https://code.obs.carnegiescience.edu/cosmos
[4] https://bitbucket.org/chil_sai/binospec

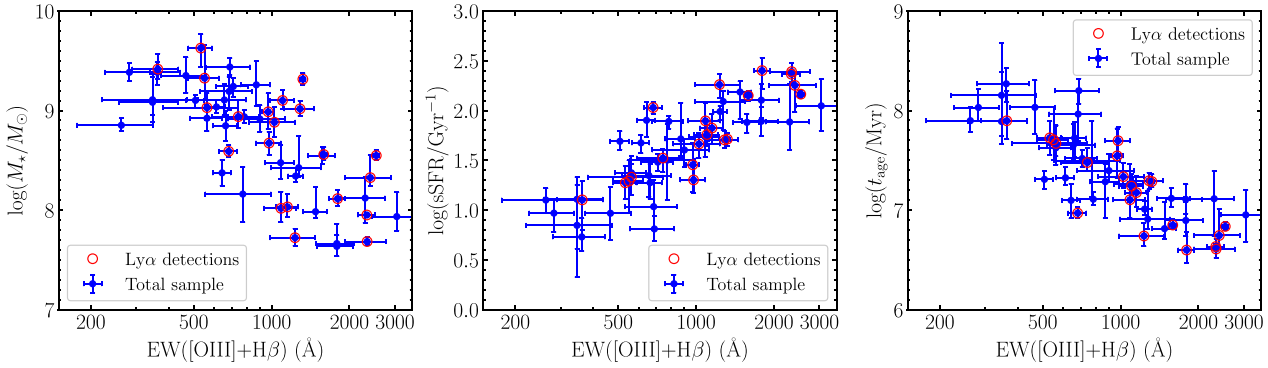

Figure 2. Stellar mass (left-hand panel), specific star formation rate (middle), and stellar age (right) as a function of [O III] + H β EW for the 49 extreme [O III] emitters at $z = 2.2$–3.7 in our spectroscopic sample. The properties are derived from photoionization modelling using BEAGLE. Galaxies with Ly α emission line measurements (S/N >3) are marked by red circles. Systems with larger [O III] + H β EWs have lower stellar masses, larger sSFRs, and younger stellar ages.

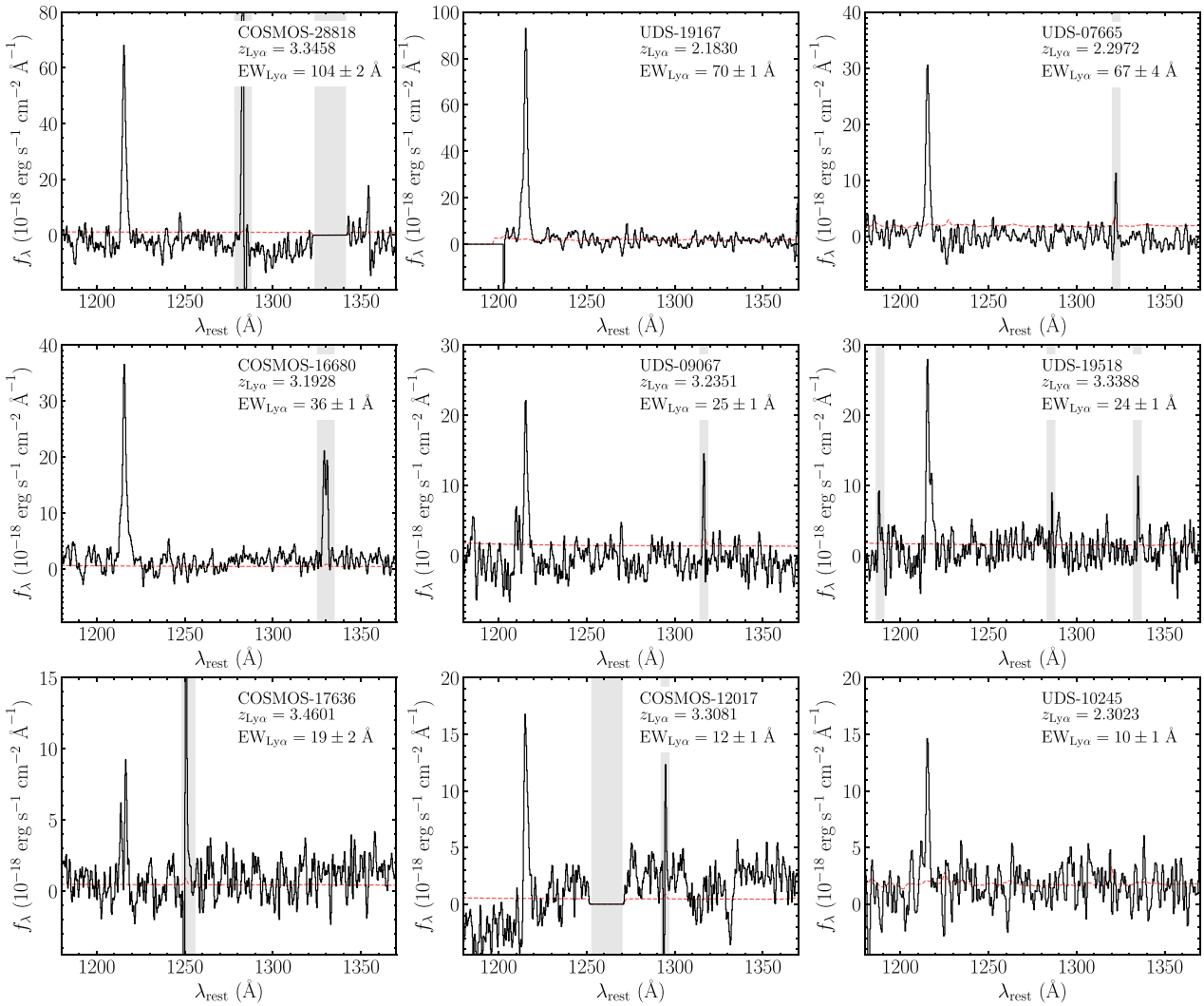

Figure 3. Examples of Ly α emission lines presented in the rest-frame UV spectra of $z = 1.3$–3.7 extreme [O III] emitters. The black solid lines and red dashed lines represent flux and error, respectively. Detected emission lines are marked by black dotted lines. The grey regions indicate gaps between spectra or wavelength ranges contaminated by sky line residuals.

Table 1. List of the 21 Ly α line emitting galaxies at $z = 2.2$–3.7 in our spectroscopic sample, including Ly α fluxes ($F_{Ly\alpha}$) and equivalent widths ($EW_{Ly\alpha}$). Systemic redshifts (z_{sys}) are computed by fitting [O III] λ5007 or O III] λ1666 emission lines.

Target	R.A. (hh:mm:ss)	Decl. (dd:mm:ss)	z_{sys}	$z_{Ly\alpha}$	$F_{Ly\alpha}$ (10^{-18} erg s^{-1} cm^{-2})	$EW_{Ly\alpha}$ (Å)	$EW_{[O III]+H\beta}$ (Å)	[O III]/[O II]
COSMOS-12017	10:00:35.387	+02:18:05.730	–	3.3081	42.21 ± 0.98	12.2 ± 0.3	532 ± 55	–
COSMOS-16680	10:00:48.029	+02:20:57.824	3.1846	3.1921	137.70 ± 1.19	36.2 ± 0.3	1102 ± 118	–
COSMOS-17636	10:00:40.510	+02:21:32.379	–	3.4601	18.92 ± 3.15	11.4 ± 1.9	562 ± 181	–
COSMOS-18503	10:00:19.083	+02:22:04.057	–	3.4229	18.90 ± 0.74	8.3 ± 0.3	744 ± 154	–
COSMOS-19118	10:00:25.726	+02:22:24.225	–	3.4268	8.44 ± 0.65	4.4 ± 0.3	363 ± 73	–
COSMOS-22402	10:00:17.831	+02:24:26.350	2.2751	2.2794	76.59 ± 7.91	26.6 ± 2.7	682 ± 45	–
COSMOS-27885	10:00:36.317	+02:28:17.384	–	2.2546	79.81 ± 11.58	48.1 ± 7.0	1087 ± 115	–
COSMOS-28818	10:00:40.009	+02:29:01.853	–	3.3458	168.80 ± 2.11	104.1 ± 1.3	2409 ± 490	–
COSMOS-31220	10:00:40.671	+02:31:00.551	–	3.4312	20.87 ± 0.78	7.6 ± 0.3	1288 ± 169	–
UDS-06274	02:17:52.310	−05:15:20.264	–	3.1040	10.00 ± 2.61	5.5 ± 1.4	550 ± 75	–
UDS-07665	02:17:33.781	−05:15:02.848	2.2955	2.2972	72.50 ± 4.39	67.7 ± 4.1	1800 ± 101	–
UDS-08078	02:17:02.741	–05:14:57.498	3.2277	3.2385	18.21 ± 2.85	4.9 ± 0.8	1321 ± 30	9.1 ± 0.5
UDS-09067	02:17:01.477	–05:14:45.359	3.2288	3.2351	53.72 ± 3.07	25.1 ± 1.4	2541 ± 63	15.3 ± 1.5
UDS-10245	02:17:22.926	–05:14:30.628	2.2995	2.3023	29.50 ± 4.10	11.0 ± 1.5	978 ± 107	8.1 ± 3.0
UDS-10805	02:17:23.712	–05:14:22.974	2.2925	2.2934	35.83 ± 5.57	27.8 ± 4.3	1232 ± 245	6.7 ± 2.9
UDS-15533	02:17:26.075	–05:13:25.277	–	2.1589	45.71 ± 7.19	20.4 ± 3.2	1152 ± 87	–
UDS-19167	02:17:43.535	–05:12:43.610	2.1833	2.1830	219.00 ± 4.67	70.9 ± 1.5	2335 ± 178	10.4 ± 2.6
UDS-19518	02:17:19.013	–05:12:38.390	3.3368	3.3388	50.51 ± 2.65	24.7 ± 1.3	970 ± 52	13.3 ± 3.8
UDS-21724	02:17:20.006	–05:12:10.624	3.2278	3.2291	26.75 ± 2.70	23.8 ± 2.4	1591 ± 51	17.0 ± 2.6
UDS-24093	02:17:51.205	–05:11:42.241	–	3.7116	23.99 ± 2.45	23.4 ± 2.4	1026 ± 208	–
UDS-29766	02:17:43.464	–05:10:33.445	2.3023	2.3041	145.70 ± 33.55	142.4 ± 32.8	2341 ± 418	10.1 ± 2.9

$z = 2.2$–2.4 galaxies is systematically lower than that in $z = 3.1-3.7$ galaxies. At $z = 2.2$–2.4, the measured Ly α emission line fluxes range from 3.0×10^{-17} erg s^{-1} cm^{-2} to 2.2×10^{-16} erg s^{-1} cm^{-2}, and the median 3σ flux limit of undetected Ly α is 6.7×10^{-17} erg s^{-1} cm^{-2}. At $z = 3.1-3.7$, the measured Ly α emission line fluxes range from 8.4×10^{-18} erg s^{-1} cm^{-2} to 1.7×10^{-16} erg s^{-1} cm^{-2}, and the median 3σ flux limit of undetected Ly α is 1.7×10^{-17} erg s^{-1} cm^{-2}.

We next compute the Ly α emission line EWs. Accurate measurement of Ly α EW is based on both the measurements of Ly α emission line flux and the underlying continuum flux density. Since many of our rest-frame UV spectra do not show high S/N (>5) continuum feature near Ly α, we take advantage of broad-band photometry from Skelton et al. (2014) to estimate the continuum flux density. We consider filters with wavelength coverage between rest-frame 1250 Å and 2600 Å (the same wavelength range used to compute UV slope in Calzetti, Kinney & Storchi-Bergmann 1994) and fit the broad-band fluxes with a power law ($f_\lambda \propto \lambda^\beta$). From the fitted $f_\lambda - \lambda$ relation, we derive the average flux density between 1225 Å and 1250 Å (Kornei et al. 2010) as the continuum flux density. The Ly α EWs are then computed by dividing the measured Ly α emission line fluxes by the continuum flux densities, ranging from 4 Å to 142 Å with a median value of 24 Å for the 21 Ly α emitting systems in our sample. Among the 21 galaxies with Ly α emission line detections, only eight are at $z = 2.2$–2.4 (out of 23 galaxies observed at this redshift). This is because Ly α is situated at the blue end of the IMACS or Binospec spectra ($\simeq$ 3890–4130 Å) where the efficiency declines rapidly ($\simeq$ 30 per cent of the maximum efficiency). For the $z = 2.2$–2.4 galaxies without Ly α detections, the median 3σ upper limit of Ly α EW is 23 Å. On the other hand, half (13 out of 26) of the $z = 3.1-3.7$ galaxies are detected with Ly α emission lines, and the median 3σ upper limit of Ly α EW for those without Ly α detections is 5 Å.

Finally, for a subset (11 out of 21) of Ly α emitting galaxies with O III] λ1666 or [O III] λ5007 emission lines (and hence systemic redshifts) measured from ground-based telescopes, we compute the velocity offset between Ly α and O III] or [O III]. The Ly α velocity offsets of these 11 sources are from −28 km/s to 766 km/s, with a median of 164 km/s. This indicates that the Ly α emission is typically redshifted with respect to oxygen emission lines, but the velocity offsets are lower than the average value (445 km/s) of more massive, typical star-forming galaxies at $z \sim 2$ (Steidel et al. 2010). In Table 1, we summarize the Ly α properties of the 21 extreme [O III] emitters with Ly α emission detections in our spectroscopic sample.

3 LYMAN-ALPHA SPECTRAL PROPERTIES OF EXTREME [O III] EMITTERS AT $z = 1.3$–3.7

In this section, we use our $z \simeq 2$–3 spectroscopic sample to quantify the dependence of the Ly α EW on [O III] + H β EW, providing a baseline for interpreting how internal galaxy properties impact the production and escape of Ly α in the population of extreme line emitters, which is common at $z > 6$. Work has previously shown that the production efficiency of hydrogen-ionizing photons increases with [O III] + H β EW (Chevallard et al. 2018, T19), suggesting that the most intense [O III] + H β emitters produce more hydrogen-ionizing photons relative to L_{UV} at 1500 Å than galaxies with lower [O III] + H β EWs. Since Ly α is powered by hydrogen-ionizing photons, we expect that the luminosity of Ly α relative to L_{UV} should also scale with [O III] + H β EW. However, the precise scaling of Ly α EW with [O III] + H β EW depends not only on Ly α production but also on the escape of Ly α through the ISM and the circumgalactic medium (CGM) of the galaxy. The large sSFRs required to produce large [O III] + H β EW could result in extreme feedback conditions that maximize the transmission of Ly α. How the ISM and CGM modulate the escape of Ly α in this class of galaxies is not well quantified in a statistical manner, making it difficult to interpret the extent to which internal galaxy properties are driving the anomalous Ly α seen in galaxies with intense [O III] emission at $z > 7$.

Our rest-frame UV spectroscopic survey of extreme [O III] emitters allows us to make progress in the determination of the Ly α EW distribution in galaxies with [O III] + H β EW >300 Å, building on

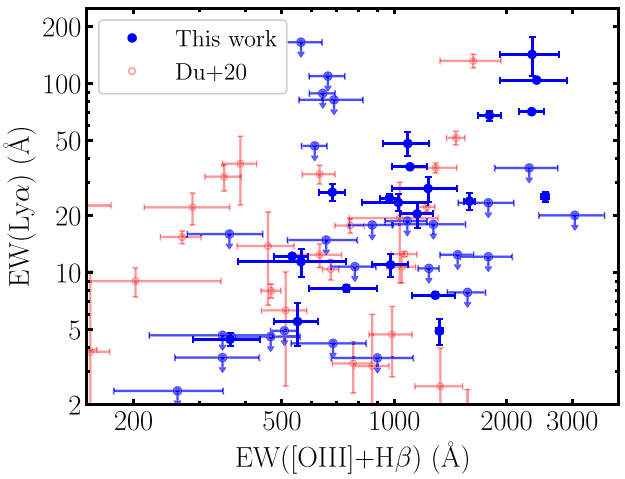

Figure 4. Ly α EW as a function of [O III] + H β EW for our sample (blue circles) and the sample in Du et al. (2020) (open red circles). Galaxies with large Ly α EW (>50 Å) are absent at [O III] + H β EW <500 Å, while this population becomes more common at [O III] + H β EW >1000 Å. Also, not all the galaxies with [O III] + H β EW >1000 Å show strong Ly α, with about half of this population showing Ly α EW <10–20 Å.

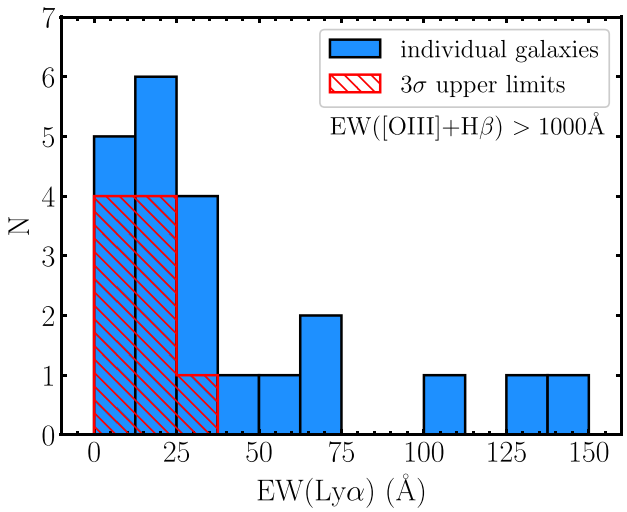

Figure 5. Ly α EW distribution of $z \sim$ 2–3 galaxies with the largest [O III] + H β EWs (>1000 Å). The data set shown in this plot combines our spectroscopic sample and the sample in Du et al. (2020). Sources with Ly α emission line detections are plotted with blue histograms. For those without significant Ly α detections, we plot the 3σ upper limits with red hatched histograms. Ly α line emission is not uniformly strong in galaxies with intense [O III] + H β line emission (EW >1000 Å); we find that 48 per cent of these systems show Ly α EW below 10–20 Å.

the recent survey presented in Du et al. (2020). We consider sources in our sample at $z = 2.2$–3.7, the redshift range where our optical spectra are able to detect Ly α emission. Our current survey contains 49 extreme [O III] emitters ($EW_{[O\,III]\lambda\lambda4959,5007} > 300$ Å or equivalently $EW_{[O\,III]+H\beta} > 340$ Å) with Ly α constraints. We have focused our survey on building the sample of galaxies with the [O III] + H β EWs (>1500 Å) exhibited by many of the known Ly α detections at $z >$ 7. We currently have obtained Ly α constraints for 11 objects with [O III] + H β EW >1500 Å.

In Fig. 4, we present the Ly α EWs of galaxies in our sample as a function of [O III] + H β EW. We present both detections and non-detections and also include the similarly selected sample from Du et al. (2020). Two things are important to take away from the data. First, we see an absence of the largest Ly α EWs (>50 Å) among the lower [O III] + H β EWs (<500 Å) in our sample. Such strong Ly α emitters appear to become more common among the most extreme [O III] + H β (EW >1000 Å), as was previously reported in several other studies (Yang et al. 2017a; Du et al. 2020). At the largest [O III] + H β EWs (>2000 Å), we start to see Ly α detections with $EW_{Ly\,\alpha} =$ 100–150 Å, requiring extremely efficient production and transmission. According to the BEAGLE photoionization models, these galaxies are dominated by light from extremely young stellar populations (<10 Myr), with low metallicities ($\simeq 0.1$–$0.2\,Z_\odot$) and large ionization parameters (log $U = -2.0$ to -1.5), as expected for a galaxy that has recently experienced a significant upturn in its star formation.

The second key takeaway from Fig. 4 is that the Ly α is not uniformly strong among galaxies with intense optical nebular line emission ($EW_{[O\,III]+H\beta} > 1000$ Å). We see relatively weak Ly α (EW <10 Å) and several non-detections in this population, suggesting significant neutral hydrogen-covering fractions. This can be more clearly seen in Fig. 5, where we show the Ly α EW distribution of galaxies with $EW_{[O\,III]+H\beta} > 1000$ Å. This plot shows that 48 per cent of these systems have relatively low Ly α EWs (<10–20 Å). Thus, at least at $z \simeq$ 2–3, it is evident that not all of the extreme [O III] + H β emitting galaxies are strong Ly α emitters. This finding was also reported in Du et al. (2020) based on very deep Keck/LRIS spectra (see red open circles in Fig. 4). Our survey extends this result to the most extreme [O III] + H β emitting galaxies. Since we expect all systems with intense optical line emission ($EW_{[O\,III]+H\beta} > 1000$ Å) to be efficient producers of Ly α (Chevallard et al. 2018, T19), the results described above suggest that many of these galaxies have their Ly α weakened within the ISM or CGM. If $z > 7$ galaxies are similar, we should not expect to see strong Ly α in every system with extreme [O III] + H β emission, as has been seen in recent reionization-era surveys (Stark et al. 2017; Endsley et al. 2021b).

Our sample allows us to investigate why some extreme [O III] emitters have strong Ly α emission and others do not. Here, we consider the seven galaxies with the most extreme optical line emission in our sample ($EW_{[O\,III]+H\beta} > 1800$ Å), corresponding to systems undergoing a rapid upturn or burst of star formation. In this subset, there are four very strong Ly α emitters (Ly α EW >50 Å) and three systems with weaker or undetected Ly α (see Fig. 6 for two examples). According to the best-fitting BEAGLE photoionization models (see Section 2.1), the four objects with strong Ly α (EW >50 Å) have similarly large sSFRs (median sSFR =239 Gyr^{-1}), large ionization parameters (median log $U = -1.83$), and low metallicities (median $Z = 0.10\,Z_\odot$) as the three systems with weaker Ly α emission (EW <50 Å, median sSFR =151 Gyr^{-1}, median log $U = -1.52$, and median $Z = 0.16\,Z_\odot$). Thus, in our current sample, we do not see substantial differences in the stellar and ionized gas properties of strong and weak Ly α emitters with $EW_{[O\,III]+H\beta} > 1800$ Å. Both populations appear to be dominated by very young and metal-poor stellar populations, suggesting broadly similar radiation fields with comparable production efficiencies of ionizing (and Ly α) photons.

What does appear different is the velocity offset of Ly α with respect to the systemic redshift ($\Delta v_{Ly\alpha}$). Considering only those systems with $EW_{[O\,III]+H\beta} > 1800$ Å, we find that the four galaxies with strong Ly α emission have systematically smaller velocity offsets ($\Delta v_{Ly\alpha} = -28$ km/s to 164 km/s, with a median value of 155 km/s) with respect to the single weaker Ly α emitter where it

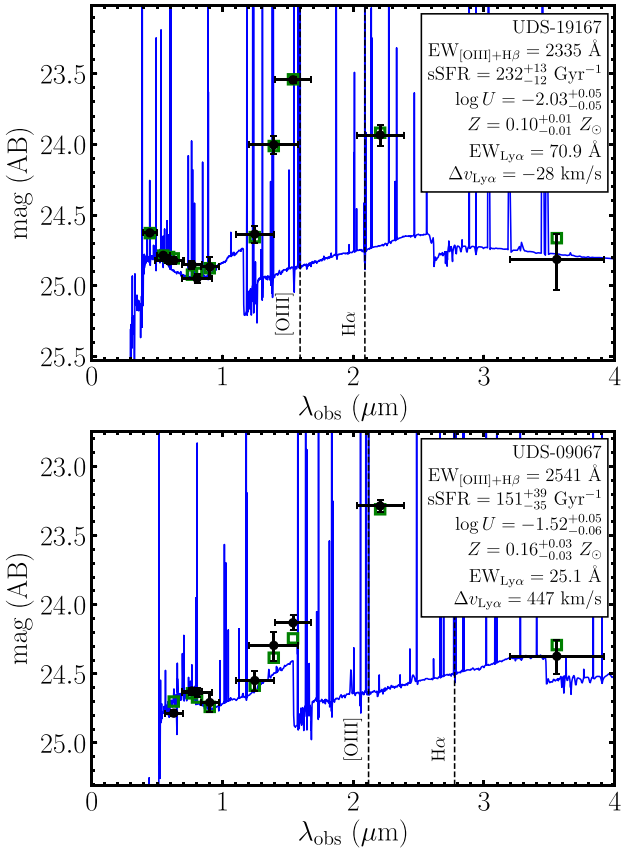

Figure 6. Broad-band SEDs of two of the most extreme [O III] emitters ($EW_{[O\,III]+H\beta}$ > 1800 Å) with Ly α emission in our sample. The two objects have similar [O III] + H β EWs but UDS-19167 (upper panel) shows a larger Ly α EW and smaller velocity offset than UDS-09067 (lower panel). Observed broad-band photometry is shown as solid black circles. The best-fitting SED models inferred from BEAGLE are plotted by solid blue lines, and synthetic photometry is presented by open green squares. We write the sSFR, the ionization parameter, and the metallicity derived from BEAGLE, as well as the [O III] + H β EW, Ly α EW, and velocity offset of each object in the upper right corner.

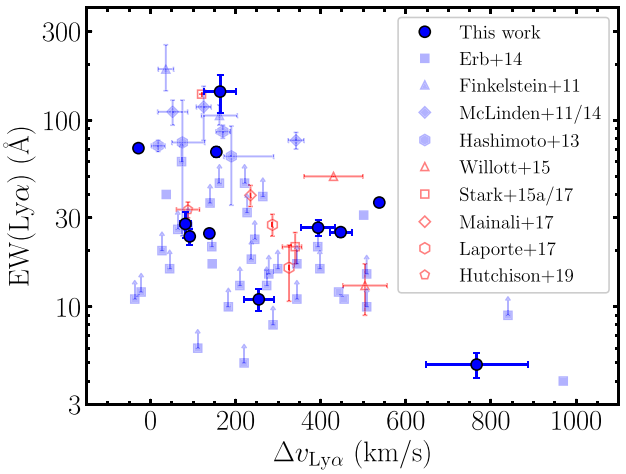

Figure 7. The relationship between the Ly α velocity offset and Ly α EW. We present velocity offsets of our sample of extreme [O III] emitters with Ly α emission with blue circles. We also show velocity offsets of $z \sim 2$–3 Ly α emitters from literature with blue solid symbols (square: Erb et al. 2014; triangle: Finkelstein et al. 2011; diamond: McLinden et al. 2011, 2014; hexagon: Hashimoto et al. 2013), and $z > 6$ Ly α emitters with red open symbols (triangle: Willott et al. 2015; square: Stark et al. 2015, 2017; diamond: Mainali et al. 2017; hexagon: Laporte et al. 2017; pentagon: Hutchison et al. 2019). It is clear that galaxies with larger Ly α EWs tend to have smaller Ly α velocity offsets.

was possible to measure a velocity offset ($\Delta v_{Ly\alpha}$ = 447 km/s), a trend that is consistent with what is seen in the broader population of star-forming galaxies at these redshifts (e.g. Finkelstein et al. 2011; McLinden et al. 2011, 2014; Hashimoto et al. 2013; Erb et al. 2014) and with our full sample of extreme line emitters with $EW_{[O\,III]+H\beta}$ = 300–1800 Å (Fig. 7). These results may reflect some combination of larger column density, covering fraction, or velocity dispersion of hydrogen near line centre in galaxies with weak Ly α emission (e.g. Erb et al. 2014). As a result, Ly α photons are forced to shift significantly in wavelength in order to escape. In these galaxies, Ly α photons diffuse spatially (often outside of the spectroscopic aperture) and face absorption by dust, both of which contribute to the weak Ly α emission. While extreme optical line emitters are often associated with strong Ly α emission (e.g. Yang et al. 2017a; Stark et al. 2017) and significant Lyman continuum (LyC) leakage (Vanzella et al. 2016, 2018; Izotov et al. 2018), the results in Fig. 7 indicate that significant hydrogen columns are often located in the vicinity of the young super star clusters powering the nebular emission.

High-resolution imaging from *HST* highlights another difference between strong and weak Ly α emitters in galaxies with extreme optical line emission. In Fig. 8, we present colour images of six of the seven galaxies in our sample with the most intense [O III] + H β emission ($EW_{[O\,III]+H\beta}$ > 1800 Å), suggesting a very recent upturn in star formation within the galaxy.[5] The three systems in the top row have strong Ly α (EW = 68–142 Å) and those in the bottom have weak or undetected Ly α (EW <35 Å). To quantify the structural parameters of these six objects, we use SExtractor (Bertin & Arnouts 1996) to measure the half-light radius ($r_{1/2}$) and the ellipticity (defined as $e = 1 - b/a$, where a and b are semimajor and semiminor axis) from *HST*/F814W (rest-frame UV) images. We find that the three strong Ly α emitters have slightly smaller radii ($r_{1/2} = 0.49^{+0.01}_{-0.04}$ kpc) comparing to the three galaxies with weaker Ly α ($r_{1/2} = 0.76^{+0.08}_{-0.09}$ kpc), consistent with previous studies indicating that galaxies with larger Ly α EWs tend to have smaller sizes (e.g. Law et al. 2012; Malhotra et al. 2012). We additionally find that strong Ly α emitters have lower ellipticities ($e = 0.17^{+0.02}_{-0.06}$) than those with weaker Ly α ($e = 0.64^{+0.00}_{-0.20}$), indicating that systems lacking strong Ly α tend to have a disc-like or irregular shape. This is consistent with results found previously for the general population of Ly α emitters at $z \sim$ 2–6 (Shibuya et al. 2014; Kobayashi et al. 2016; Paulino-Afonso et al. 2018). It has been suggested previously that the range of observed ellipticities may be related to the inclination angle of the galaxy (Verhamme et al. 2012; Paulino-Afonso et al. 2018). In this context, the variation of Ly α EW in the most extreme [O III] emitters could be explained as an effect of viewing angle, with Ly α photons tending to escape face-on (i.e. low ellipticity) following the path of least opacity as suggested by simulations (e.g. Verhamme et al. 2012; Behrens & Braun 2014). However, it is not clear that the population of extreme line emitters has the same disc-like morphology simulated in these studies, so the inclination explanation should be treated with some

[5]While there are seven galaxies in our sample with $EW_{[O\,III]+H\beta}$ > 1800 Å, only six have *HST*/ACS imaging.

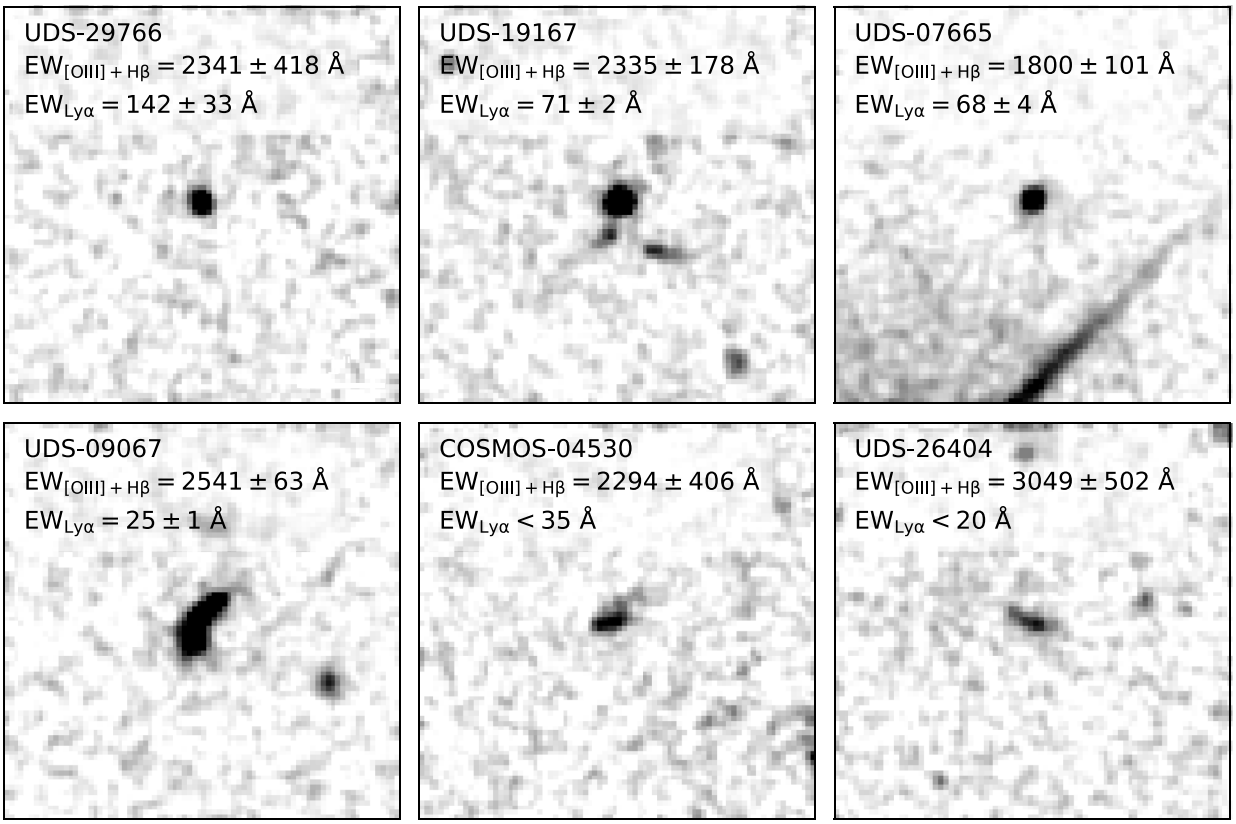

Figure 8. *HST*/ACS F814W postage stamps ($5'' \times 5''$ with pixel scale of $0''.06$) of six galaxies with the largest [O III] + Hβ EWs (>1800 Å) in our $z \simeq 2$–3 spectroscopic sample. The upper panels show images of three objects with strong Lyα emission (EW >50 Å). These galaxies are characterized by a round shape with low ellipticity ($e = 0.11-0.19$). The lower panels show images of other three galaxies with weaker or non-detected Lyα (EW <50 Å). They show irregular or disc-like morphology with much larger ellipticity ($e = 0.44$–0.64).

caution. Regardless of the precise explanation, these results suggest that the subset of the extreme [O III] emitting population that appears irregular or disc-like is likely to have sufficient hydrogen covering fractions to weaken Lyα emission.

In the final portion of this section, we now seek to provide a baseline for comparison against similar measurements in the reionization era. We derive the Lyα emitter fraction ($x_{Ly\alpha}$) as a function of [O III] + Hβ EW at $z \simeq 2$–3. We consider three different [O III] + Hβ EW bins (300–600 Å, 600–900 Å, and 900–3000 Å). To optimize comparison with $z > 7$ samples, we consider only galaxies with $-21.75 < M_{UV} < -20.25$. Since previous studies show that the Lyα fraction strongly depends on UV luminosity (Stark et al. 2010), this control will help to isolate the dependence of Lyα on the [O III] + Hβ EW. With our M_{UV} selection applied, we have 9, 6, and 10 objects with $EW_{[O\,III]+H\beta}$ = 300–600 Å, =600–900 Å, and =900–3000 Å. We compute the fraction of galaxies in each bin with Lyα EW >25 Å, including both detections and non-detections with robust (<25 Å) upper limits. We find that the fraction of galaxies with $EW_{Ly\alpha} > 25$ Å increases with [O III] + Hβ EW at 2σ significance, from $x_{Ly\alpha} = 0.00^{+0.18}_{-0.00}$ to $0.17^{+0.29}_{-0.14}$ and $0.40^{+0.20}_{-0.18}$ at $EW_{[O\,III]+H\beta}$ = 300–600 Å, 600–900 Å, and 900–3000 Å. We note that the sample size of bright ($-21.75 < M_{UV} < -20.25$) extreme [O III] emitters at $z \sim 2$–3 is relatively small ($\lesssim$10 per [O III] + Hβ EW bin), which is due to the low number density of this population ($\lesssim$10 per 120 arcmin^2). In the future, we aim to obtain a larger sample to improve the statistics. Since the Lyα fraction closely tracks the UV continuum slope (e.g. Stark et al. 2010), we also consider the effects of limiting our measurement to those objects with blue UV slopes ($\beta < -1.8$) similar to those seen at $z > 7$. The same trend emerges, albeit with a slightly larger Lyα fraction ($0.50^{+0.22}_{-0.22}$) in the bin with largest [O III] + Hβ EW.

The results presented above indicate the manner in which Lyα EWs increase with [O III] + Hβ EWs at $z \simeq 2$–3, building on results previously presented in Du et al. (2020). Whether this is driven entirely by the increase in the production efficiency of ionizing photons (and hence likely the Lyα production efficiency) in extreme optical line emitters is not clear. To explore this, we derive the Lyα escape fraction as a function of [O III] + Hβ EW for the galaxies in our sample. The Lyα escape fraction ($f_{esc}^{Ly\alpha}$) is defined as the ratio of the observed Lyα luminosity to the intrinsic Lyα luminosity. To compute the intrinsic Lyα luminosity, we follow an approach very similar to what has been done previously in the literature (e.g. Hayes et al. 2010; Erb et al. 2014; Henry et al. 2015; Trainor et al. 2015; Verhamme et al. 2017; Yang et al. 2017a; Jaskot et al. 2019). We assume the Lyα/Hα flux ratio expected by Case B recombination (8.7; see Henry et al. 2015 for discussion about the Lyα/Hα flux ratio) and compute the Lyα escape fraction using the following equation: $f_{esc}^{Ly\alpha} = F_{Ly\alpha}^{obs}/(8.7 \times F_{H\alpha}^{corrected})$. For galaxies with H$\alpha$ detections, we use the measured Hα fluxes (T19). Otherwise, we use the Hα fluxes inferred from the best-fitting photoionization models. To verify that the Hα flux predicted by the models is robust, we compare the model Hα flux and the observed Hα flux for the subset of galaxies with Hα detections. The results reveal good agreement, with a median error of only 2.5 per cent, smaller than

the observed uncertainties in the Hα flux (median uncertainty of 4 per cent). We perform the dust correction to the Hα flux assuming the Calzetti et al. (2000) attenuation law, consistent with previous studies of Lyα escape fraction (e.g. Hayes et al. 2010; Henry et al. 2015; Yang et al. 2017a).

For the 21 galaxies with Lyα detections in our sample, we find that the Lyα escape fraction increases with [O III] + Hβ EW. The median $f_{\rm esc}^{\rm Ly\alpha}$ increases from 0.02 $\pm$ 0.01 at EW$_{\rm [O\,III]+H\beta}$ = 300–600 Å (3 sources) to 0.03 $\pm$ 0.01, 0.06 $\pm$ 0.01, and 0.11 $\pm$ 0.03 at EW$_{\rm [O\,III]+H\beta}$ = 600–900 Å (three sources), 900–1500 Å (nine sources), and >1500 Å (six sources), respectively. This relationship suggests that the increase of Lyα EW with [O III] + Hβ EW is driven by not only the increase in the Lyα production efficiency but also the enhanced transmission of Lyα photons through the ISM and the CGM in extreme [O III] emitters. Physically, this may indicate that when galaxies go through periods of high sSFR, the feedback associated with the recent burst is able to disrupt the surrounding gas sufficiently to boost the transfer of Lyα photons. We can also quantify the dependence of the Lyα escape fraction on the Lyα EW in our sample. We find that the escape fraction increases with Lyα EW, with values of $f_{\rm esc}^{\rm Ly\alpha} \simeq 0.02$ at EW$_{\rm Ly\alpha}$ < 10 Å to $f_{\rm esc}^{\rm Ly\alpha} \simeq 0.30$ at EW$_{\rm Ly\alpha}$ > 100 Å. The trend we derived here is consistent with the EW$_{\rm Ly\alpha}$ versus $f_{\rm esc}^{\rm Ly\alpha}$ relation inferred from observations of both local and high-redshift galaxies (e.g. Verhamme et al. 2017; Yang et al. 2017a; Jaskot et al. 2019), consistent with the picture whereby large Lyα EW traces large Lyα escape fraction. We note that in addition to the Lyα production efficiency and the Lyα escape fraction, the Lyα EWs are also affected by the absorption of ionizing photons by dust in the ionized gas (Charlot & Fall 2000). However, because the dust attenuation in the extreme emission line galaxies tends not to be significant (Tang et al. 2019), this effect is minimal for the galaxies considered here. Indeed our best-fitting photoionization models predict that dust absorption of ionizing photons reduces the Balmer lines by only 12 per cent on average. As a result, the increase of Lyα EW with [O III] + Hβ EW is mainly dominated by the increase of Lyα production efficiency and Lyα escape fraction.

4 DISCUSSION

The results described in Section 3 provide a $z \simeq 2$–3 framework for understanding the Lyα properties of galaxies expected to be typical in the reionization era. Here, we consider implications for the large Lyα detection rates in $z > 7$ galaxies with strong [O III] + Hβ emission (Section 4.1) and for the ionizing efficiency of this population (Section 4.2).

4.1 Implications for the Lyα visibility at $z > 7$

The evolving visibility of Lyα emission from star-forming galaxies at $z > 6.5$ remains one of our primary observational probes of the progress of reionization, implying IGM neutral fractions in excess of $x_{\rm HI} > 0.76$ (68 per cent confidence) at $z \simeq 8$ (e.g. Mason et al. 2019). The detection of Lyα in 100 per cent of the galaxies in RB16 (each selected to have strong [O III] + Hβ emission) stands in striking contrast to the strong line attenuation experienced by most $z \simeq 7$–9 galaxies. Why the RB16 objects are detectable in Lyα at redshifts where the IGM is thought to be mostly neutral is not clear. The Lyα statistics presented in Section 3 provide the baseline at $z \simeq 2$–3 necessary to understand these results and the implications they have for the factors regulating the visibility of Lyα in reionization-era galaxies.

While the optical line EWs of the RB16 galaxies are extremely large (EW$_{\rm [O\,III]+H\beta}$ = 900–2000 Å; c.f. Roberts-Borsani, Ellis & Laporte 2020), so are those of typical galaxies (EW$_{\rm [O\,III]+H\beta}$ = 670 Å; Labbé et al. 2013) that generally do not show Lyα at $z > 7$. If the detectability of Lyα in the RB16 galaxies is primarily driven by the radiation field associated with the intense [O III] + Hβ line emission, it therefore suggests a substantial change in the Lyα EW distribution at EW$_{\rm [O\,III]+H\beta}$ > 900 Å. Our survey suggests that such a trend does indeed exist at $z \simeq 2$–3, building on previous findings in Du et al. (2020). Our data indicate that the Lyα emitter fraction (EW$_{\rm Ly\alpha}$ > 25 Å) in luminous ($M_{\rm UV} < -20.25$) and blue ($\beta < -1.8$) galaxies increases by roughly 3× (at 2σ significance) between [O III] + Hβ EW = 600–900 Å and 900–3000 Å. In Section 3, we demonstrated that this trend can be explained by a shift towards larger ionizing photon production efficiency and larger Lyα escape fractions in galaxies with extreme [O III] + Hβ emission. These extreme line emitters are those with the largest sSFR (Fig. 2), as expected for systems undergoing a burst or upturn in star formation. During this presumably brief phase, the Lyα emission is enhanced relative to galaxies with lower sSFR. Thus, by selecting $z \simeq 7$–8 galaxies with the largest [O III] + Hβ EWs (e.g. RB16), one is more likely to select galaxies with Lyα emission above current sensitivity limits.

While such extreme [O III] + Hβ emitters are very rare at $z \simeq 2$–3, they become increasingly more commonplace in the reionization era (Smit et al. 2015; De Barros et al. 2019; Endsley et al. 2021a), reflecting a shift towards larger sSFRs at earlier times. Indeed, in a given sample of $z \simeq 7$–8 galaxies, the [O III] + Hβ EWs can be expected to span from 300 Å to 3000 Å (Endsley et al. 2021a). As can be seen in Fig. 4, this range will show large variations in Lyα EW that have nothing to do with the IGM, with the most extreme optical line emitters much more likely to show strong Lyα emission. The dependence of Lyα on [O III] + Hβ EW must be considered when using the evolving Lyα properties as a probe of reionization. Recent spectroscopic investigations at $z > 6.5$ have often prioritized sources with large IRAC excesses (and hence large [O III] + Hβ EW) as these objects have narrow confidence intervals on their photometric redshifts, allowing Lyα to be placed in regions where atmospheric transmission is large. While this increases the likelihood of a meaningful constraint on Lyα, it also increases the likelihood that Lyα will have an atypically large EW, biasing inferences on the Lyα EW distribution. These problems can be mitigated in future surveys by targeting galaxies with representative values of [O III] + Hβ EW, while also taking efforts to match galaxies across redshift with similar Lyα production efficiencies.

4.2 Implications for ionizing photon escape from extreme [O III] emitters

Recent studies have suggested that the extreme optical line emitting galaxies may be very effective ionizing agents. Not only do they have large ionizing production efficiencies (Chevallard et al. 2018, T19) but they also may often leak significant fractions of their ionizing radiation into the IGM. This latter finding has come to light from rest-frame optical spectra of galaxies at $z \simeq 0.1 - 0.3$ and $z \simeq 3$ known to be LyC leakers (e.g. Izotov et al. 2016; Izotov, Thuan & Guseva 2017; Izotov et al. 2018; Fletcher et al. 2019; Vanzella et al. 2020). In these existing samples, the largest escape fractions are commonly associated with very large rest-frame optical line EWs ([O III] + Hβ EW >1000–2000 Å), indicating a population of galaxies that has recently experienced a burst or upturn in star formation. These objects also tend to show very large ratios of their [O III] to [O II] emission lines (hereafter O32) (Faisst 2016; Izotov et al. 2016; Fletcher et al. 2019; Vanzella et al. 2020), perhaps indicating reduced [O II]

emission stemming from density-bounded H II regions (Jaskot & Oey 2013; Nakajima & Ouchi 2014) or large ionization parameters (see Plat et al. 2019). Collectively, these observations suggest that when galaxies undergo intense bursts of star formation, the conditions are often met for LyC leakage. However, it has recently become clear that intense rest-frame optical nebular emission and large O32 are not sufficient criteria to guarantee LyC leakage (e.g. Izotov et al. 2018; Jaskot et al. 2019; Nakajima et al. 2020), potentially indicating that a subset of systems undergoing bursts has significant hydrogen columns that completely cover the young stars along the line of sight (see also Katz et al. 2020; Barrow et al. 2020). The impact of neutral gas on LyC escape can be studied indirectly via resonant emission lines (i.e. Ly α, Mg II) or interstellar absorption lines. Galaxies with gas conditions favourable to LyC leakage (e.g. low column density, low gas-covering fraction) show strong Ly α with narrow-line profiles (e.g. Verhamme et al. 2015; Dijkstra, Gronke & Venkatesan 2016; Steidel et al. 2018; Rivera-Thorsen et al. 2019), optically thin Mg II emission profiles (Henry et al. 2018; Chisholm et al. 2020), and weak interstellar absorption lines from low ionization metals (Reddy et al. 2016; Steidel et al. 2018).

As our understanding of the conditions required for LyC leakage improves, it so becomes possible to explore whether those conditions are met in a large fraction of $z > 7$ galaxies. The first step towards this goal has been realized through characterization of the [O III] + H β strengths at $z \simeq 7$ (Labbé et al. 2013; Smit et al. 2014). These results indicate that extreme optical line emission is much more common at $z \simeq 7$ than at lower redshifts (De Barros et al. 2019; Endsley et al. 2021a). *JWST* will soon complement these studies with measurements of O32. If extreme line emitters at $z \simeq 7$ are similar to those at $z \simeq 0$–3, we expect the O32 values to be uniformly large (i.e. O32 > 6–10) in the subset of the population with [O III] + H β EW in excess of 1000 Å (T19). Taken together, these results suggest that a sizeable fraction of the reionization-era population is likely to have rest-frame optical spectral properties very similar to many of the known LyC leakers at $z \simeq 0$–3. But as discussed above, large O32 and intense optical line emission do not guarantee leakage, as many of these bursts are covered by large enough columns of hydrogen to absorb the escaping ionizing radiation. Ideally, Ly α emission line spectra could be used to inform the range of line-of-sight neutral hydrogen opacities in galaxies at $z \simeq 7$ (Matthee et al. 2018), but at such high redshifts, these efforts are complicated by the impact of the partially neutral IGM on Ly α. So in practice, attempts to study Ly α properties in extreme optical line emitting galaxies (and implications for LyC escape) are best conducted at redshifts after reionization, systematically characterizing the statistics of Ly α in galaxies matched to the sSFRs that appears common at $z \simeq 7$.

The spectra described in this paper allow us to take a step in this direction, quantifying the frequency with which $z \simeq 2$–3 extreme emission line galaxies have Ly α properties that appear required for LyC leakage. These efforts build on studies at $z \simeq 0$ (Jaskot et al. 2019; Izotov et al. 2020) and at $z \simeq 2$–3 (Du et al. 2020). While our eventual goal is to provide a large enough sample to provide a statistical measure of the Ly α line profiles as a function of rest-frame optical line EWs (or effectively the sSFR), here we first consider implications of trends between Ly α EW and the [O III] + H β EW. We are primarily interested in galaxies with [O III] + H β EW >900 Å, as these are the systems that have the very large O32 ratios (>6; T19) and large star formation rate surface densities that appear frequently linked to efficient ionizing photon escape (e.g. Izotov et al. 2018; Vanzella et al. 2020; Naidu et al. 2020). The results described in Section 3 provide two key insights into the Ly α properties of this population.

The spectroscopic sample indicates that very large EW Ly α becomes more common in the most extreme optical line emitters, consistent with results from nearby galaxies (Yang et al. 2017a). At high redshift, this was previously hinted at in the analysis of Du et al. (2020). They found that Ly α becomes prominent (>20 Å) only at extremely strong [O III] emission ($EW_{[O\,III]\lambda\lambda4959,5007} > 1000$ Å, or equivalently $EW_{[O\,III]\lambda5007} > 750$ Å) displaying no apparent correlation at lower [O III] EWs. Our sample extends this analysis to higher optical line EWs, adding Ly α constraints on 11 galaxies with [O III] λ5007 EW >1000 Å to the two systems satisfying these criteria in Du et al. (2020). This [O III] EW threshold corresponds to [O III] + H β EW >1500 Å, implying a population with extremely large sSFR (>100 Gyr^{-1}; Fig. 2). In this subset, we begin to see extremely strong Ly α emission, with some galaxies reaching upwards of Ly α EW = 70–150 Å. These systems have both efficient Ly α production and low enough neutral hydrogen opacities along the line of sight to facilitate large escape fractions of Ly α (see Section 3). Looking at the entire sample with [O III] + H β EW >1500 Å, we find that 50 per cent have Ly α EW >25 Å, and 38 per cent have Ly α EW >50 Å, both of which are much larger than found in more typical systems at these redshifts. These objects appear to be ideal candidates for significant escape fractions, with similar rest-frame UV and rest-frame optical spectroscopic properties as many of the known LyC leakers. Physically, these results emphasize the importance of strong bursts (as indicated by extreme nebular line EWs) in creating the conditions that appear linked to ionizing photon escape.

While Ly α is on average more prominent in galaxies with extreme optical line emission, it is not uniformly strong in this population. As is clear from above, roughly half of galaxies with sSFR in excess of 100 Gyr^{-1} have weak (<25 Å) Ly α (see Table 1). These sources tend to have larger Ly α velocity offsets with respect to systemic, implying a substantial covering fraction of neutral hydrogen at similar velocity as the young star clusters. This subset of extreme optical line emitters is not likely to leak ionizing radiation along the line of sight. From *HST* imaging, we see that the extreme [O III] emitters with weaker Ly α tend to appear more disc-like or irregular (Fig. 8). Taken at face value, these results suggest that when extreme emission line galaxies appear elongated in high-resolution imaging, they are more likely to have large enough hydrogen-covering fractions to reduce the transmission of Ly α (and LyC) emission. It is conceivable that these objects may be more likely to transmit a larger fraction of their Ly α (or LyC) emission if viewed along one of their shorter axes. Such viewing angle effects are commonly predicted in simulations (Ma et al. 2020; Katz et al. 2020; Barrow et al. 2020) but remain challenging to directly confirm observationally.

Overall, the results presented here provide continued support for indications that the extreme optical line emitting galaxies ([O III] + H β EW >900 Å) are very effective ionizing agents. While such objects are rare at $z \simeq 0$–3, they become more common in the $z > 7$ population (Smit et al. 2014, 2015; De Barros et al. 2019; Endsley et al. 2021a). This reflects an overall shift towards more rapidly rising star formation histories at $z > 6$, with the systems having the largest sSFRs capable of powering the nebular line emission described here. In the future, higher spectral resolution observations should be able to characterize the distribution of Ly α line profiles as a function of [O III] + H β EW, providing more direct constraints on the likelihood of leaking ionizing radiation (e.g. Rivera-Thorsen et al. 2017). Meanwhile, as larger samples of extreme [O III] emitters lacking Ly α are obtained, we should be able to improve our understanding of why some systems undergoing rapid upturns in star formation are more efficient than others at clearing channels for ionizing photons to escape.

5 SUMMARY

We present Ly α EW measurements of 49 extreme optical line emitting galaxies at $z = 2.2$–3.7 with $EW_{[O\,III]+H\beta} = 300$–$3000$ Å, similar to the range of optical line EWs seen in reionization-era galaxies and building on previous work presented in Du et al. (2020). The sample includes 11 sources with the largest [O III] + H β EWs (>1500 Å) that characterize many of the known Ly α emitters at $z > 7$ (e.g. RB16), enlarging the Ly α statistics for the most extreme [O III] emitters at $z \simeq 2$–3 by a factor of 5. Our data provide an empirical baseline at where the IGM is mostly ionized, allowing us to investigate how factors internal to galaxies impact the Ly α visibility (or lack thereof) in reionization-era galaxies, especially the anomalously large Ly α detection rate of the most extreme [O III] line emitting systems at $z > 7$ (Stark et al. 2017). We summarize the results below:

(1) We measure the Ly α EW for the 49 extreme [O III] emitters at $z = 2.2$–3.7 in our spectroscopic sample. We find that the fraction of strong Ly α emitters ($EW_{Ly\alpha} > 25$ Å) scales with the rest-frame optical emission line EW. Considering galaxies in our sample with similar UV luminosities ($-21.75 < M_{UV} < -20.25$) and blue UV slopes ($\beta < -1.8$) as the $z > 7$ objects in RB16, the Ly α emitter fraction ($x_{Ly\alpha} = 0.50$) of galaxies with $EW_{[O\,III]+H\beta} > 900$ Å (the values probed by RB16) is $\sim 3\times$ larger than that ($x_{Ly\alpha} = 0.20$) of galaxies with $EW_{[O\,III]+H\beta}$ (=600–900 Å). One of the primary factors driving this trend is the harder radiation field in more intense [O III] emitters (T19), leading to larger Ly α production efficiencies. We find that the transmission of Ly α through the ISM and CGM is also likely to increase with $EW_{[O\,III]+H\beta}$, perhaps reflecting the more intense feedback experienced during the extreme star formation episodes that are associated with large optical line EWs.

(2) We present the Ly α EW distribution of galaxies with very large [O III] + H β EWs (>1000 Å) in our sample. Although the fraction of strong Ly α emitter reaches the largest values at these [O III] + H β EWs, the emerging data set suggests that $\sim$50 per cent of these systems show relatively low Ly α EWs (<10–20 Å). Since galaxies with $EW_{[O\,III]+H\beta} > 1000$ Å are found to be very efficient in producing hydrogen ionizing photons (and hence Ly α photons) (T19), the weak Ly α emission likely points to reduced transmission through the ISM and CGM. This result suggests that not all galaxies experiencing a burst or upturn in star formation have cleared pathways allowing Ly α (or LyC) emission to escape.

(3) To understand why some galaxies undergoing bursts have conditions that facilitate the escape of Ly α and others do not, we explore the properties of galaxies in our sample with the most extreme optical line emission ($EW_{[O\,III]+H\beta} > 1800$ Å). We find that those systems that are weaker in Ly α tend to have morphologies with larger ellipticities ($e = 0.44$–0.64) than those with strong Ly α emission ($e = 0.11 - 0.19$), suggesting that the weak Ly α emitters in this sample of extreme line emitters tend to appear more disc-like or elongated than those with strong Ly α emission. This finding is similar to results seen in the more general population of Ly α emitters (Shibuya et al. 2014; Kobayashi et al. 2016; Paulino-Afonso et al. 2018). If the ellipticity is set by the observed inclination, extreme line emitters with weak Ly α are most likely to be observed along their longer axis (i.e. edge-on), and those with strong Ly α tend to be seen face-on, similar to predictions from simulations (Verhamme et al. 2012; Behrens & Braun 2014). These results suggest significant line-of-sight differences in the Ly α opacity through extreme line emitting galaxies.

(4) We discuss implications of our survey for the findings of RB16, where luminous $z \simeq 7$–9 galaxies with extremely large [O III] + H β EWs are seen with much stronger Ly α emission than the general population at $z > 7$ ($EW_{[O\,III]+H\beta} \sim 670$ Å). For the $z \sim 2$–3 sample, the fraction of Ly α emitters (EW >25 Å) among luminous ($M_{UV} < -20.25$) and blue ($\beta < -1.8$) galaxies increases by $3\times$ (at 2σ significance) from $EW_{[O\,III]+H\beta} = 600$–$900$ Å to $EW_{[O\,III]+H\beta} = 900$–$3000$ Å. This trend can be explained by a shift towards both enhanced ionizing photon (and hence Ly α) production efficiency and Ly α escape fraction in galaxies with larger sSFRs (and hence larger [O III] + H β EWs). These results help explain that by selecting galaxies with the largest [O III] + H β EWs, one is more likely to select galaxies with detectable large EW Ly α emission.

(5) We discuss the implications for LyC leakage in extreme [O III] emitters. Previous work has indicated that this population has uniform large O32 values (T19), similar to those seen in many galaxies with large escape fractions. Overall, the results continue supporting the picture that the most extreme optical line emitting galaxies, which become more common at $z > 7$, are very effective ionizing agents. Future observations with higher spectral resolution will help to characterize the Ly α emission line profile and provide more direct constraints on LyC leakage.

ACKNOWLEDGEMENTS

We are grateful for enlightening conversations with John Chisholm and Xiaohui Fan. RE acknowledges funding from JWST/NIRCam contract to the University of Arizona, NAS5-02015. EC acknowledges support from ANID project Basal AFB-170002. This work is based on observations taken by the 3D-HST Treasury Program (GO 12177 and 12328) with the NASA/ESA *HST*, which is operated by the Association of Universities for Research in Astronomy, Inc., under NASA contract NAS5-26555. Observations reported here were obtained from the Magellan Telescopes located at Las Campanas Observatory, Chile, and the MMT Observatory, a joint facility of the University of Arizona and the Smithsonian Institution. This paper uses data products produced by the OIR Telescope Data Center, supported by the Smithsonian Astrophysical Observatory. We acknowledge the MMT queue observers for assisting with MMT/Binospec observations.

This research made use of ASTROPY, a community-developed core PYTHON package for Astronomy (Astropy Collaboration 2013), NUMPY, SCIPY (Jones et al. 2001), and MATPLOTLIB (Hunter 2007).

DATA AVAILABILITY

The data underlying this article will be shared on reasonable request to the corresponding author.

REFERENCES

Amorín R. et al., 2014, A&A, 568, L8
Amorín R. et al., 2015, A&A, 578, A105
Astropy Collaboration, 2013, A&A, 558, A33
Atek H. et al., 2011, ApJ, 743, 121
Barkana R., Loeb A., 2004, ApJ, 609, 474
Barrow K. S. S., Robertson B. E., Ellis R. S., Nakajima K., Saxena A., Stark D. P., Tang M., 2020, ApJ, 902, L39
Behrens C., Braun H., 2014, A&A, 572, A74
Bertin E., Arnouts S., 1996, A&AS, 117, 393
Bouwens R. J., Illingworth G. D., Oesch P. A., Caruana J., Holwerda B., Smit R., Wilkins S., 2015, ApJ, 811, 140
Calzetti D., Kinney A. L., Storchi-Bergmann T., 1994, ApJ, 429, 582
Calzetti D., Armus L., Bohlin R. C., Kinney A. L., Koornneef J., Storchi-Bergmann T., 2000, ApJ, 533, 682

Cardamone C. et al., 2009, MNRAS, 399, 1191
Caruana J., Bunker A. J., Wilkins S. M., Stanway E. R., Lorenzoni S., Jarvis M. J., Ebert H., 2014, MNRAS, 443, 2831
Charlot S., Fall S. M., 2000, ApJ, 539, 718
Chevallard J., Charlot S., 2016, MNRAS, 462, 1415
Chevallard J. et al., 2018, MNRAS, 479, 3264
Chisholm J., Prochaska J. X., Schaerer D., Gazagnes S., Henry A., 2020, MNRAS, 498, 2554
Cowie L. L., Barger A. J., Hu E. M., 2011, ApJ, 738, 136
Dayal P., Ferrara A., 2018, Phys. Rep., 780, 1
De Barros S., Oesch P. A., Labbé I., Stefanon M., González V., Smit R., Bouwens R. J., Illingworth G. D., 2019, MNRAS, 489, 2355
Dijkstra M., 2014, PASA, 31, e040
Dijkstra M., Gronke M., Venkatesan A., 2016, ApJ, 828, 71
Dressler A. et al., 2011, PASP, 123, 288
Du X., Shapley A. E., Tang M., Stark D. P., Martin C. L., Mobasher B., Topping M. W., Chevallard J., 2020, ApJ, 890, 65
Endsley R., Stark D. P., Chevallard J., Charlot S., 2021a, MNRAS, 500, 5229
Endsley R., Stark D. P., Charlot S., Chevallard J., Robertson B., Bouwens R. J., Stefanon M., 2021b, MNRAS, tmp, 470E
Erb D. K. et al., 2014, ApJ, 795, 33
Fabricant D. et al., 2019, PASP, 131, 075004
Faisst A. L., 2016, ApJ, 829, 99
Fan X. et al., 2001, AJ, 121, 54
Fan X. et al., 2006, AJ, 132, 117
Finkelstein S. L. et al., 2011, ApJ, 729, 140
Finkelstein S. L. et al., 2013, Nature, 502, 524
Fletcher T. J., Tang M., Robertson B. E., Nakajima K., Ellis R. S., Stark D. P., Inoue A., 2019, ApJ, 878, 87
Fontana A. et al., 2010, ApJ, 725, L205
Forrest B. et al., 2017, ApJ, 838, L12
Hashimoto T., Ouchi M., Shimasaku K., Ono Y., Nakajima K., Rauch M., Lee J., Okamura S., 2013, ApJ, 765, 70
Hayes M. et al., 2010, Nature, 464, 562
Henry A., Scarlata C., Martin C. L., Erb D., 2015, ApJ, 809, 19
Henry A., Berg D. A., Scarlata C., Verhamme A., Erb D., 2018, ApJ, 855, 96
Hoag A. et al., 2019, ApJ, 878, 12
Hu E. M., Cowie L. L., Barger A. J., Capak P., Kakazu Y., Trouille L., 2010, ApJ, 725, 394
Huang X. et al., 2015, ApJ, 801, 12
Hunter J. D., 2007, Comput. Sci. Eng., 9, 90
Hutchison T. A. et al., 2019, ApJ, 879, 70
Izotov Y. I., Schaerer D., Thuan T. X., Worseck G., Guseva N. G., Orlitová I., Verhamme A., 2016, MNRAS, 461, 3683
Izotov Y. I., Thuan T. X., Guseva N. G., 2017, MNRAS, 471, 548
Izotov Y. I., Worseck G., Schaerer D., Guseva N. G., Thuan T. X., Fricke Verhamme A., Orlitová I., 2018, MNRAS, 478, 4851
Izotov Y. I., Schaerer D., Worseck G., Verhamme A., Guseva N. G., Thuan T. X., Orlitová I., Fricke K. J., 2020, MNRAS, 491, 468
Jaskot A. E., Oey M. S., 2013, ApJ, 766, 91
Jaskot A. E., Dowd T., Oey M. S., Scarlata C., McKinney J., 2019, ApJ, 885, 96
Jones E., Oliphant T., Peterson P. et al., 2001, SciPy: Open source scientific tools for Python. Available at http://www.scipy.org/
Jung I. et al., 2018, ApJ, 864, 103
Jung I. et al., 2020, ApJ, 904, 144
Kansky J. et al., 2019, trophysics Source Code Library, record ascl:1905.004
Kashikawa N. et al., 2011, ApJ, 734, 119
Katz H. et al., 2020, MNRAS, 498, 164
Kobayashi M. A. R. et al., 2016, ApJ, 819, 25
Konno A. et al., 2014, ApJ, 797, 16
Kornei K. A., Shapley A. E., Erb D. K., Steidel C. C., Reddy N. A., Pettini M., Bogosavljević M., 2010, ApJ, 711, 693
Labbé I. et al., 2013, ApJ, 777, L19
Laporte N., Nakajima K., Ellis R. S., Zitrin A., Stark D. P., Mainali R., Roberts-Borsani G. W., 2017, ApJ, 851, 40
Law D. R., Steidel C. C., Shapley A. E., Nagy S. R., Reddy N. A., Erb D. K., 2012, ApJ, 759, 29
Loeb A., Barkana R., 2001, ARA&A, 39, 19
Ma X., Quataert E., Wetzel A., Hopkins P. F., Faucher-Giguére C.-A., Kereš D., 2020, MNRAS, 498, 2001
Madau P., Haardt F., 2015, ApJ, 813, L8
Mainali R., Kollmeier J. A., Stark D. P., Simcoe R. A., Walth G., Newman A. B., Miller D. R., 2017, ApJ, 836, L14
Malhotra S., Rhoads J. E., 2004, ApJ, 617, L5
Malhotra S., Rhoads J. E., Finkelstein S. L., Hathi N., Nilsson K., McLinden E., Pirzkal N., 2012, ApJ, 750, L36
Manti S., Gallerani S., Ferrara A., Greig B., Feruglio C., 2017, MNRAS, 466, 1160
Maseda M. V. et al., 2014, ApJ, 791, 17
Mason C. A., Treu T., Dijkstra M., Mesinger A., Trenti M., Pentericci L., de Barros S., Vanzella E., 2018, ApJ, 856, 2
Mason C. A. et al., 2019, MNRAS, 485, 3947
Matthee J., Sobral D., Gronke M., Paulino-Afonso A., Stefanon M., Röttgering H., 2018, A&A, 619, A136
McGreer I. D., Mesinger A., D'Odorico V., 2015, MNRAS, 447, 499
McLinden E. M. et al., 2011, ApJ, 730, 136
McLinden E. M., Rhoads J. E., Malhotra S., Finkelstein S. L., Richardson M. L. A., Smith B., Tilvi V. S., 2014, MNRAS, 439, 446
Mesinger A., Furlanetto S. R., 2008, MNRAS, 386, 1990
Mesinger A., Aykutalp A., Vanzella E., Pentericci L., Ferrara A., Dijkstra M., 2015, MNRAS, 446, 566
Miralda-Escudé J., 1998, ApJ, 501, 15
Momcheva I. G. et al., 2016, ApJS, 225, 27
Naidu R. P., Tacchella S., Mason C. A., Bose S., Oesch P. A., Conroy C., 2020, ApJ, 892, 109
Nakajima K., Ouchi M., 2014, MNRAS, 442, 900
Nakajima K., Ellis R. S., Robertson B. E., Tang M., Stark D. P., 2020, ApJ, 889, 161
Oemler A., Clardy K., Kelson D., Walth G., Villanueva E., 2017, Astrophysics Source Code Library, record ascl:1705.001
Oesch P. A. et al., 2015, ApJ, 804, L30
Oke J. B., Gunn J. E., 1983, ApJ, 266, 713
Ono Y. et al., 2012, ApJ, 744, 83
Ota K. et al., 2017, ApJ, 844, 85
Ouchi M. et al., 2010, ApJ, 723, 869
Ouchi M., Ono Y., Shibuya T., 2020, ARA&A, 58, 617
Paulino-Afonso A. et al., 2018, MNRAS, 476, 5479
Pentericci L. et al., 2014, ApJ, 793, 113
Planck Collaboration VI, 2018, A&A, 641, A6
Plat A., Charlot S., Bruzual G., Feltre A., Vidal-García A., Morisset C., Chevallard J., Todt H., 2019, MNRAS, 490, 978
Reddy N. A., Steidel C. C., Pettini M., Bogosavljević M., Shapley A. E., 2016, ApJ, 828, 108
Rivera-Thorsen T. E., Östlin G., Hayes M., Puschnig J., 2017, ApJ, 837, 29
Rivera-Thorsen T. E. et al., 2019, Science, 366, 738
Roberts-Borsani G. W. et al., 2016, ApJ, 823, 143 (RB16)
Roberts-Borsani G. W., Ellis R. S., Laporte N., 2020, MNRAS, 497, 3440
Robertson B. E. et al., 2013, ApJ, 768, 71
Robertson B. E., Ellis R. S., Furlanetto S. R., Dunlop J. S., 2015, ApJ, 802, L19
Santos M. R., 2004, MNRAS, 349, 1137
Santos S., Sobral D., Matthee J., 2016, MNRAS, 463, 1678
Schenker M. A., Ellis R. S., Konidaris N. P., Stark D. P., 2014, ApJ, 795, 20
Senchyna P. et al., 2017, MNRAS, 472, 2608
Shibuya T., Ouchi M., Nakajima K., Yuma S., Hashimoto T., Shimasaku K., Mori M., Umemura M., 2014, ApJ, 785, 64
Skelton R. E. et al., 2014, ApJS, 214, 24
Smit R. et al., 2014, ApJ, 784, 58
Smit R. et al., 2015, ApJ, 801, 122
Stark D. P., 2016, ARA&A, 54, 761
Stark D. P., Ellis R. S., Chiu K., Ouchi M., Bunker A., 2010, MNRAS, 408, 1628
Stark D. P., Ellis R. S., Ouchi M., 2011, ApJ, 728, L2
Stark D. P. et al., 2015, MNRAS, 450, 1846
Stark D. P. et al., 2017, MNRAS, 464, 469

Steidel C. C., Erb D. K., Shapley A. E., Pettini M., Reddy N., Bogosavljević M., Rudie G. C., Rakic O., 2010, ApJ, 717, 289
Steidel C. C., Bogosavljević M., Shapley A. E., Reddy N. A., Rudie G. C., Pettini M., Trainor R. F., Strom A. L., 2018, ApJ, 869, 123
Tang M., Stark D. P., Chevallard J., Charlot S., 2019, MNRAS, 489, 2572 (T19)
Tang M., Stark D. P., Chevallard J., Charlot S., Endsley R., Congiu E., 2021, MNRAS, 501, 3238 (T21)
Tilvi V. et al., 2014, ApJ, 794, 5
Trainor R. F., Steidel C. C., Strom A. L., Rudie G. C., 2015, ApJ, 809, 89
Treu T., Schmidt K. B., Trenti M., Bradley L. D., Stiavelli M., 2013, ApJ, 775, L29
van der Wel A. et al., 2011, ApJ, 742, 111
Vanzella E. et al., 2016, ApJ, 821, L27
Vanzella E. et al., 2018, MNRAS, 476, L15
Vanzella E. et al., 2020, MNRAS, 491, 1093
Verhamme A., Dubois Y., Blaizot J., Garel T., Bacon R., Devriendt J., Guiderdoni B., Slyz A., 2012, A&A, 546, A111
Verhamme A., Orlitová I., Schaerer D., Hayes M., 2015, A&A, 578, A7
Verhamme A., Orlitová I., Schaerer D., Izotov Y., Worseck G., Thuan T. X., Guseva N., 2017, A&A, 597, A13
Whitler L. R., Mason C. A., Ren K., Dijkstra M., Mesinger A., Pentericci L., Trenti M., Treu T., 2020, MNRAS, 495, 3602
Willott C. J., Carilli C. L., Wagg J., Wang R., 2015, ApJ, 807, 180
Yang H. et al., 2017a, ApJ, 844, 171
Yang H., Malhotra S., Rhoads J. E., Wang J., 2017b, ApJ, 847, 38
Zheng Z.-Y. et al., 2017, ApJ, 842, L22
Zitrin A. et al., 2015, ApJ, 810, L12

This paper has been typeset from a TEX/LATEX file prepared by the author.